



1 **A consistent ocean oxygen profile dataset with new quality control and bias assessment**

2

3 Viktor Gourteski<sup>1</sup>, Lijing Cheng<sup>1</sup>, Juan Du<sup>1</sup>, Xiaogang Xing<sup>2</sup>, Fei Chai<sup>3,4</sup>

4 <sup>1</sup>Institute of Atmospheric Physics, Chinese Academy of Sciences, Beijing, China

5 <sup>2</sup>State Key Laboratory of Satellite Ocean Environment Dynamics, Second Institute of Oceanography, Ministry of  
6 Natural Resources, Hangzhou, China

7 <sup>3</sup>State Key Laboratory of Marine Environmental Science, Xiamen University, Xiamen, China

8 <sup>4</sup>College of Ocean and Earth Sciences, Xiamen University, Xiamen, China

9

10 *Correspondence to:* Viktor Gouretski ([viktor.gouretski@posteo.de](mailto:viktor.gouretski@posteo.de));

11 Lijing Cheng ([chenglij@mail.iap.ac.cn](mailto:chenglij@mail.iap.ac.cn))

12

13

14 **Abstract.** The global ocean oxygen levels have declined in the past decades, posing threats to marine life and human  
15 society. High-quality and bias-free observations are crucial to understanding the ocean oxygen changes and assessing  
16 their impact. Here, we propose a new automated quality control procedure for ocean profile oxygen data. This  
17 procedure consists of a suite of nine quality checks, with outlier rejection thresholds being defined based on underlying  
18 statistics of the data. The procedure is applied to three main instrumentation types: bottle casts, CTD (Conductivity-  
19 Temperature-Depth) casts, and Argo profiling floats. Application of the quality control procedure to several manually  
20 quality-controlled datasets of good quality suggests the ability of the scheme to successfully identify outliers in the data.  
21 Collocated quality-controlled oxygen profiles obtained utilizing the Winkler titration method are used as unbiased  
22 references to estimate possible residual biases in the oxygen sensor data. The residual bias is negligible for  
23 electrochemical sensors typically used on CTD casts. We explain this as the consequence of adjusting to the concurrent  
24 sample Winkler data. However, our analysis finds a prevailing negative residual bias for the delayed-mode quality-  
25 controlled adjusted Argo profiling floats varying from -4 to -1  $\mu\text{mol kg}^{-1}$  among the data adjusted by different Argo data  
26 assembly centers (DACs). The respective overall DAC-specific corrections are suggested. Applying the new QC  
27 procedure and bias adjustment resulted in a new global ocean oxygen dataset from 1920 to 2022 with consistent data  
28 quality across bottle samples, CTD casts, and Argo floats. The adjusted Argo profile data is available at the Marine  
29 Science Data Center of the Chinese Academy of Sciences (Gouretski et al., 2023,  
30 <http://dx.doi.org/10.12157/IOCAS.20231208.001>)

31

32 **1 Introduction**

33 Progressive warming caused by the human-induced increase of the greenhouse gases in the Earth's atmosphere leads to  
34 the decline of the dissolved oxygen concentration in the global ocean because of the reduction in oxygen solubility, the  
35 increase in stratification which hampers the exchange between the surface layer and the ocean interior, and the  
36 accompanying change of ocean circulation (Keeling et al., 2010; Gregoire et al., 2021). Another factor related to human  
37 activities is the increasing input of nutrients from agriculture and wastewater. Nutrients facilitate a dense growth of  
38 phytoplankton and microbes subsequently decrease of oxygen after the phytoplankton dies. Recognizing the crucial role  
39 of dissolved oxygen for marine aerobic organisms, oceanographers started to measure oxygen in the late 19<sup>th</sup> century



40 using the chemical method developed by Winkler (1888). Since then, Winkler titration has been a standard method  
41 used on oceanographic ships and in laboratories (Langdon, 2010), and the technique has an accuracy estimated to be  
42 0.1% or  $\pm 0.3 \mu\text{mol kg}^{-1}$  (Carpenter, 1965).

43  
44 With the rapid technological progress during the 1960-70s and the development of the electronic CTD (Conductivity-  
45 Temperature-Depth) profilers, the first electrochemical sensors appeared, providing the possibility for continuous  
46 oxygen profiling, which is not possible with the Winkler method restricted by water samples from several depth levels.  
47 Electrochemical sensors are based on a Clark polarographic membrane (Clark et al., 1953). Oxygen concentration  
48 outside the membrane and oxygen diffusion through the membrane determine the sensor response. Electrochemical  
49 Clark-type sensors possess a very fast time response ( $< 1 \text{ s}$ ), with an initial accuracy of 2% of oxygen saturation and  
50 precision of about  $1 \mu\text{mol kg}^{-1}$  (Coppola et al., 2013). Sensor drift due to membrane fouling and changes in electrolyte  
51 over time requires periodic calibration. The first type of sensors applied on Biogeochemical Argo profiling floats (BGC  
52 floats) were Clark-type electrodes (Riser and Johnson, 2008).

53       Optical oxygen sensors called “optodes” are based on the principle of fluorescence quenching of a fluorescent  
54 indicator embedded in a sensing foil (Körtzinger et al. 2005, Tengberg et al., 2006). The optode sensors appeared soon  
55 after the first implementation of the Clark-type sensors on Argo floats. Compared to electrochemical sensors, optodes are  
56 characterized by long-term stability and high precision with the disadvantage of a slower response time. During the  
57 initial period of several years both Clarke-type and optode sensors were used on Argo floats (Claustre et al., 2020).  
58 However drift and initial calibration issues with electrochemical sensors has lead to the increased implementation of  
59 optodes on Argo floats (Claustre et al., 2020), for which calibration using simultaneous water samples is not possible.

60       Different techniques have been applied in the past to collect ocean oxygen data, and the total number of  
61 oxygen profile data reached a total of more than 1.2 million until 2023. However, there are a lot of data quality issues in  
62 the historical oxygen database due to many reasons, including instrumental errors, data collection failure, data  
63 processing errors, improper sample storage, unit conversion and others. These quality issues impede the various  
64 applications of oxygen data, for instance, investigating how much oxygen the ocean has lost in the past decades  
65 (Gregoire et al., 2021). Furthermore, as different instruments have different data quality, merging different  
66 instrumentation types into an integrated database requires a proof of data consistency.

67       To provide a quality-consistent database for oxygen, this study presents an automated quality control procedure  
68 for ocean oxygen profiles and analyzes the quality of oxygen data obtained by different instrumentation types. We  
69 further assess remaining oxygen biases for CTD and Argo oxygen profiles, comparing them with the reference bottle  
70 sample data obtained through Winkler method. The rest of the paper is organized as follows. The data and methods  
71 employed in the study are presented in Section 2. The data quality-control procedure is introduced in Section 3, with the  
72 data quality assessment presented in Section 4. Results of the benchmarking of the automated quality control procedure  
73 using manually controlled datasets is shown in Section 5. Assessment of the residual bias for Argo and CTD profiles is  
74 conducted in Section 6. Data availability is described in Section 7. The results of the study are summarized and  
75 discussed in Section 8.

## 76 2       Global archive of dissolved oxygen profiles

77 For the current study we used data from two large depositories: 1) World Ocean Database (as of January 2023); 2)  
78 Oxygen profiles from the Argo Global Assembly Center (GDAC) (ARGO, 2000). The WOD Argo profiles represent a  
79 blend of not-adjusted (real-time) and adjusted (delayed-mode) profiles, whereas for the data from GDACs it is possible



80 to discriminated between adjusted and unadjusted profiles. For this reason, the analysis of biases for Argo data is based  
81 on the data from the Argo GDAC.

82  
83

#### 84 2.1 Oxygen profiles from the World Ocean Database and DACs

85 World Ocean Database (Boyer et al., 2018) represents the largest depository of the dissolved oxygen profile data, which  
86 is composed of three main instrumentation types: 1) Ocean Station Data (OSD), 2) high-resolution CTD profiles, and 3)  
87 Argo profiling float (PFL) data. OSD instrumentation group is represented by bottle casts with oxygen determined by  
88 the Winkler method. CTD profiles are obtained mainly through the electrochemical sensors, whereas Argo float profiles  
89 contain data mainly obtained by optodes. The total number of profiles from all three platforms exceeds 1.2 million from  
90 1920 to 2022, so a manual quality control of the global oxygen dataset is nearly impossible.

91

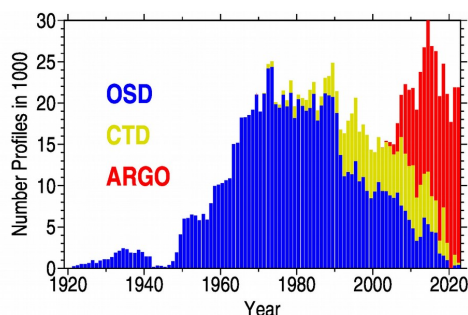


**Figure 1. Yearly number of oxygen profiles from the World Ocean Database (OSD and CTD profiles) and from national DACs.**

92 The OSD profiles are most abundant between 1960s to 2000s, CTD profiles between 1990s to 2010s, and Argo  
93 profiles dominate after 2010 (Fig. 1). The geographical distribution of oxygen profiles is inhomogeneous (Fig. 2). The  
94 OSD profiles exhibit considerably better sampling compared to CTD and Argo, with dense sampling in near-coastal  
95 areas and a sparser sampling in the central parts of the oceans (Fig. 2a). The CTD profiles are limited to transoceanic  
96 sections, leaving large data gaps especially in the central regions of Pacific, Indian, and Southern oceans (Fig. 2b).  
97 Oxygen profiles from ten national Argo DACs have been used for the current study, with the number of profiles given  
98 in Table 1. The most considerable contribution comes from two DACs: Atlantic Oceanographic and Meteorological  
99 Laboratory (AOML) and French CORIOLIS Center (Coriolis). Together these two DACs contribute with 71% of all  
100 oxygen profiles. The global sampling by Argo floats is characterized by big gaps in the tropical belt of the World Ocean  
101 (Fig. 2c) and in the marginal seas with shallow bottom depth.

102  
103

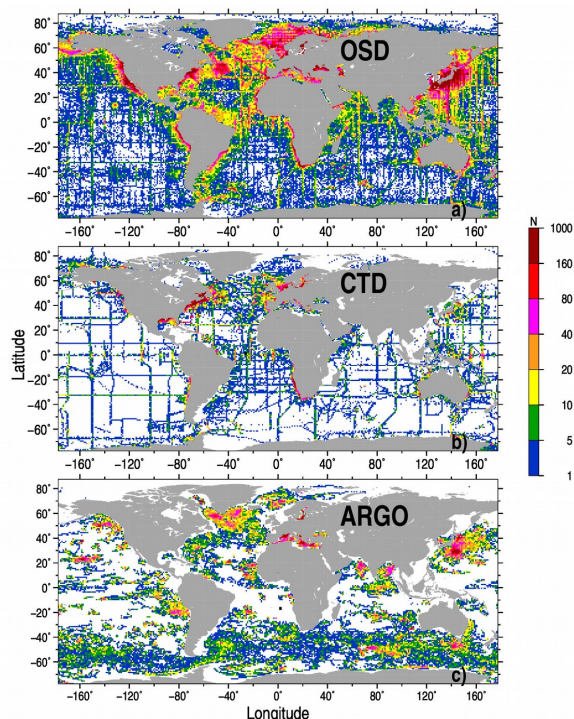


Figure 2 Number of profiles (N) in  $1^{\circ} \times 1^{\circ}$  latitude/longitude squares for OSD (a), CTD (b), and Argo (c) data

104

105 The DACs report oxygen data along with quality flags set after the quality control procedure performed in each  
106 DAC. Spatial distribution of the profiles from each DAC is shown in Fig. 3. Only the AOML dataset is characterized by  
107 a more or less global coverage. The profiles from the second large Coriolis dataset are concentrated mostly in the  
108 Atlantic and Southern oceans. Other DACs are characterized by a regional scope: JMA data come from the Pacific  
109 Ocean east of Japan, CSIRO profiles cover the Southern Ocean, CSIO mainly provides profiles in the subtropical and  
110 tropical western Pacific Ocean, BODC profiles are located in the Atlantic Ocean. Profiles from KORDI and KMA, the  
111 smallest two datasets, are concentrated in the southern part of the Sea of Japan.

### 112 3 Data quality control

113 Quality evaluation of hydrographic data typically consists of two parts: data quality control for random errors and  
114 evaluation of systematic errors or biases. These two issues often are treated separately but both essentially represent the  
115 entire quality control procedure. A unified quality control procedure has yet to be suggested for the global archive of  
116 oxygen profile data, and oxygen-related studies often rely on WOD (Garcia et al., 2018) and Argo (Thierry et al., 2021)  
117 quality control procedures. The efforts undertaken under the IQuOD initiative (Cowley, 2021) resulted in a  
118 comprehensive study where different quality control procedures for temperature profiles were compared and evaluated  
119 (Good et al., 2022). As shown in the previous section, the characteristic feature of the global oxygen data archive is its  
120 heterogeneity. In the early years, a relatively small amount of data permitted expert quality control, but for the actual  
121 global archive automated quality control procedures (AutoQC) are required.

122



123

124

125 **Table 1.** Argo oxygen profiles from different national DACs

N	National Data Assembly Center	Code Name	Number of Argo profiles	Number of Argo profiles collocated with Winkler profiles	Percent of Argo profiles having collocations with Winkler profiles
1	Atlantic Oceanographic and Meteorological Laboratory, US	AOML	89059	32396	41.08
2	CORIOLIS data Center, France	Coriolis	63220	33233	65.09
3	Commonwealth Scientific and Industrial Research Organisation, Australia	CSIRO	19183	3302	23.75
4	Japan Meteorological Agency, Japan	JMA	15981	11233	82.90
5	Indian National Centre for Ocean Information Services, India	INCOIS	9901	2069	33.09
6	Second Institute of Oceanography, Ministry of Natural Resources, China	CSIO	6455	3921	68.98
7	Marine Environmental Data Service, Canada	MEDS	4605	14.04	50.50
8	British Oceanographic Data Center, UK	BODC	3533	1905	61.57
9	Korea Ocean Research and Development Institute, Korea	KORDI	2239	0	0
10	Korea Meteorological Administration, Korea	KMA	93	0	0

126

127 The AutoQC procedure aims to identify and flag outliers, which represent observations significantly deviating  
 128 from the majority of other data in the population. Monhor and Takemoto (2005) noted that there is no rigid  
 129 mathematical definition of an outlier. The outliers do not necessarily represent erroneous data and can occur due to the  
 130 natural variability of the measured variable. A quality control procedure defines outliers using a set of thresholds, which  
 131 are based on physical laws (for instance, the maximum solubility of gases in the water) or are defined based on the  
 132 statistical properties of the data population.

133 To increase the reliability in detecting erroneous data a set of quality-checks is applied to each profile. The  
 134 larger the number of failed distinct quality checks, the higher the probability that the flagged observation represents a  
 135 data outlier. Based on the available quality control schemes for oceanographic data (most of them were developed for  
 136 temperature and/or salinity profiles) quality checks can be subdivided into the following groups:

137

138

139

140

141

142

143

144

145

1. Check of location, date and bottom depth of the profile.
2. Check of profile attributes (maximum sampled depth, number of levels, variables measured) correspond to the attributes of the instrumentation type.
3. Range check, e.g. comparison of observations at each level against minimum/maximum value thresholds, which are set for the entire ocean, oceanic basin (global ranges) or for the particular location and depth (local ranges).
4. Check of the profile shape, which is characterized by the vertical gradient of the measured variable at observed levels, by the number of local extrema, and by the presence of spikes.



146

147

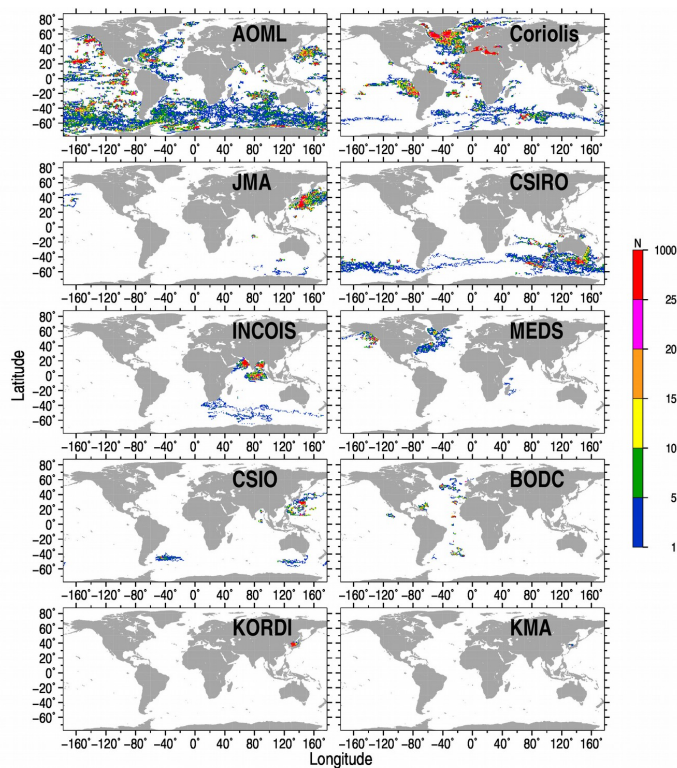


**Figure 3.** The number (N) of oxygen profiles in  $1^\circ \times 1^\circ$  spatial boxes for different DACs. The name of each DAC is shown on Asia.

148 Quality control procedures often assume Gaussian distribution law, and outliers are defined in terms of  
149 multiple times the standard deviation from the mean value (Z-score method). However, distributions of oceanographic  
150 parameters are typically skewed, and the assumption of Gaussian distribution leads to false data rejection. Hubert and  
151 Vandervieren (2008) developed the adjusted Tukey's boxplot method for skewed distribution with a more accurate  
152 representation of possible outliers. Following this approach, Gouretski (2018) and Tan et al. (2023) applied quality  
153 control checks taking into account skewness of temperature distribution.

154 Developing the quality control procedure which consists of a suite of distinct checks we assume that oxygen  
155 data obtained by the reference Winkler method are superior in their quality compared to the sensor data. For this reason,  
156 we use OSD oxygen profiles in order to set the local accepted oxygen ranges at depth levels. In several other quality  
157 checks, instrument-dependent thresholds are used. There are a total of nine distinct quality checks which are introduced  
158 in the following sections.

### 159 3.1 Geographical Location Check

160 One possible indication of an erroneous geographical profile location can be the case when the depth of the deepest  
161 profile measurement exceeds the local ocean bottom depth. We use GEBCO 0.5-minute resolution digital bathymetry



162 map to define thresholds for this check. For each 0.1x0.1-degree grid node the difference between the maximum  
163 GEBCO depth within the 111km radius and the grid-node GEBCO depth is calculated (Fig. 4). If the difference between  
164 the deepest profile measurement depth and the local GEBCO depth exceeds the threshold the geographical location of  
165 the profile is considered to be in error and data at all levels are flagged.

166

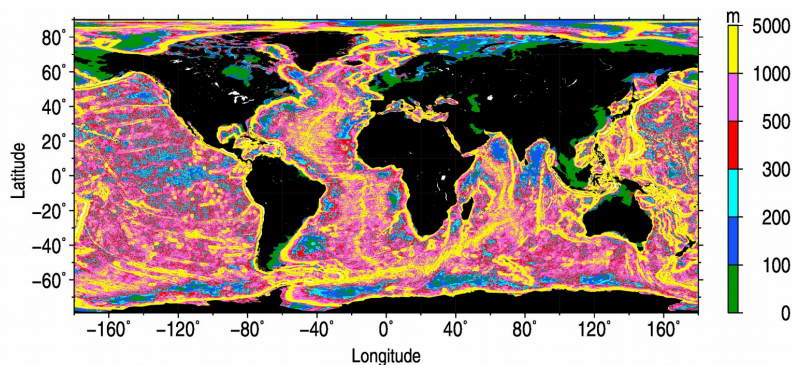


**Figure 4. Threshold (in meters) for the difference between the profile's deepest sample depth and the local GEBCO bottom depth.**

167

### 168 3.2 Crude range check

169 The test is applied to identify observations that are grossly in error (the so-called 'blunders') (Fig. 5). These data  
170 correspond to the cases of the total instrumentation fault or crude errors introduced during the data recording or  
171 formatting. The overall minimum/maximum oxygen ranges are defined based on the entire archive of the OSD profiles.  
172 These overall ranges are set both for depth levels and for temperature surfaces, because the maximum oxygen solubility  
173 depends on temperature. The relative frequencies serve as guidance to produce the overall oxygen minimum and  
174 maximum limits, which approximately correspond to the relative frequency of 0.05%.

175

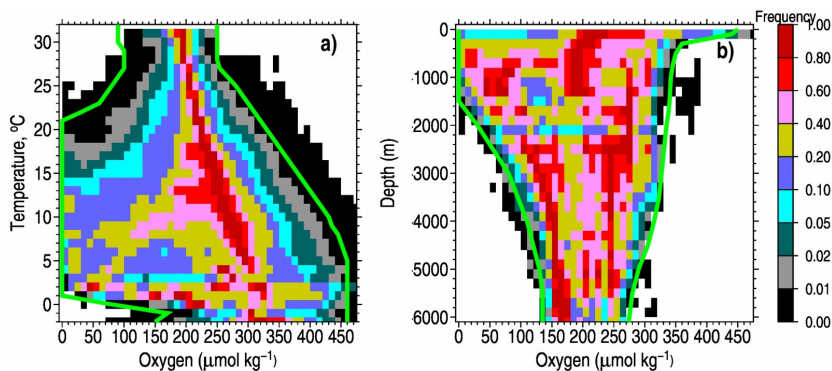


**Figure 5. Normalized oxygen histograms used to define overall oxygen ranges versus temperature (a) and versus depth (b). Minimum and maximum overall oxygen limits are shown by solid green lines.**

176

177



### 178 3.3 Maximum oxygen solubility check

179 According to Henry's law, the quantity of an ideal gas that dissolves in a definite volume of liquid is directly  
180 proportional to the partial pressure of the gas. It is also known that gas solubility in the water typically decreases with  
181 increasing temperature. However, in the photic layer of the ocean, oxygen is produced by phytoplankton through  
182 photosynthesis so that oxygen supersaturation can evolve. Oxygen production due to photosynthesis leads to the  
183 formation of small bubbles (10-70 micron) with increasing oxygen supersaturation accompanied by a higher number of  
184 bubbles and their shift towards large sizes (Marks, 2008). Another factor leading to oversaturation is the inaccurate  
185 taking of oxygen samples accompanied by the building of air bubbles.

186

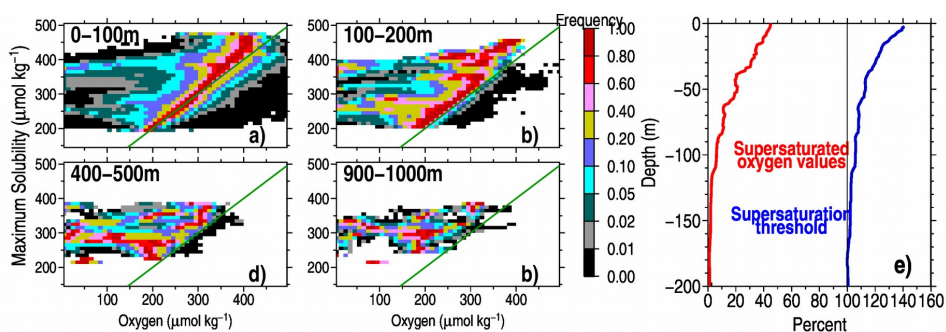


**Figure 6. Supersaturation check: a-d) normalized frequency histograms between maximum solubility and the dissolved oxygen for different layers. Bin size is  $10 \mu\text{mol kg}^{-1}$ ; e) percent of supersaturated oxygen values (red) and threshold percent for supersaturation applied in the quality control procedure.**

187

188 Histograms in Fig. 6a-c show frequency for different values of observed oxygen concentration ( $C_{\text{obs}}$ ) and  
189 maximum oxygen solubility ( $C_{\text{max}}$ ) for given temperature and salinity. For each maximum solubility bin, the  
190 frequencies are normalized by the number of the values in the most populated bin. The distribution mode for the layer  
191 0-100m (Fig. 6a) follows the line  $C_{\text{obs}}=C_{\text{max}}$  progressively deviating to lower values above  $300 \mu\text{mol kg}^{-1}$ . The diagram  
192 shows that a significant number of observed oxygen concentration values in this layer exceeds the maximum solubility.  
193 In the deeper layers (Fig. 6 b-d), the number of cases with supersaturation decreases. As illustrated by Fig. 6 e, the  
194 percentage of supersaturated values decreases from about 42 % in the near-surface layer to about 0.0% below the 200 m  
195 level. We used accumulated versions of the above histograms to put the supersaturation percent threshold (Fig. 6e) at  
196 each level above 200 m by 99-th quantile. Below 200 m all supersaturated oxygen values are flagged.

### 197 3.4 Stucked value check

198 Malfunctioning of sensors often results in stucked values when the same oxygen concentration is reported for all or  
199 most of the observed levels. To identify such profiles, we calculated oxygen standard deviations for each oxygen profile  
200 to build histograms (Fig. 7) for each instrumentation type. Only profiles with at least five oxygen levels are considered.  
201 Unlike the OSD and Argo data, for which the frequency of profiles drops for low standard deviation values, the CTD  
202 profiles are characterized by a distinct peak for the lowest standard deviation values. Guided by Fig. 7 we set the  
203 thresholds of  $4 \mu\text{mol kg}^{-1}$  and  $1 \mu\text{mol kg}^{-1}$  and for CTD and PFL profiles respectively, respectively. No thresholds are  
204 applied for OSD profiles, as stucked values are characteristics of the electronic sensors only.





205 **3.5 Spike check**

206 Spikes are the data at levels that strongly deviate from those at neighboring levels. For each observed level  $z_k$ , the test  
 207 value  $s = s_1 - s_2$  is calculated, where  $s_1 = |p_k - 0.5(p_{k-1} + p_{k+1})|$ ,  $s_2 = |0.5(p_{k+1} - p_{k-1})|$  and  $p$  denotes the oxygen value. The  
 208 observation is identified as outliers when  $s$  exceeds a threshold value. Due to the larger natural oxygen variability in the  
 209 upper layers, we set depth-dependent spike thresholds using the respective accumulated spike frequency histograms.  
 210 Shown in Fig. 8a-b are histograms for two layers, and the entire threshold profile is shown in the Fig. 8c. Spike  
 211 threshold corresponds to the 99.8% frequency.

212

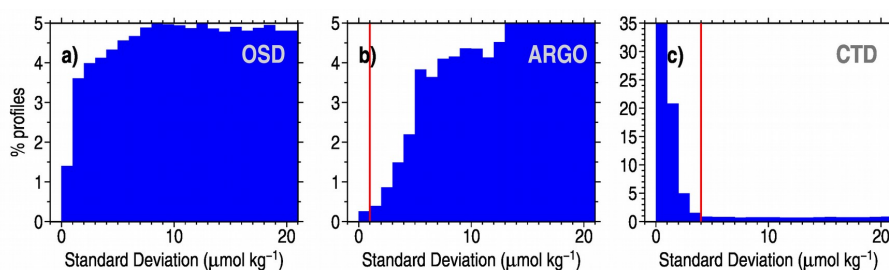


**Figure 7. Oxygen profile standard deviation for OSD (a), Argo (b), and CTD (c) instrumentation types. Only profiles with at least five levels of oxygen data are considered. Red vertical lines show the respective threshold values for ARGO and CTD profiles.**

213

214

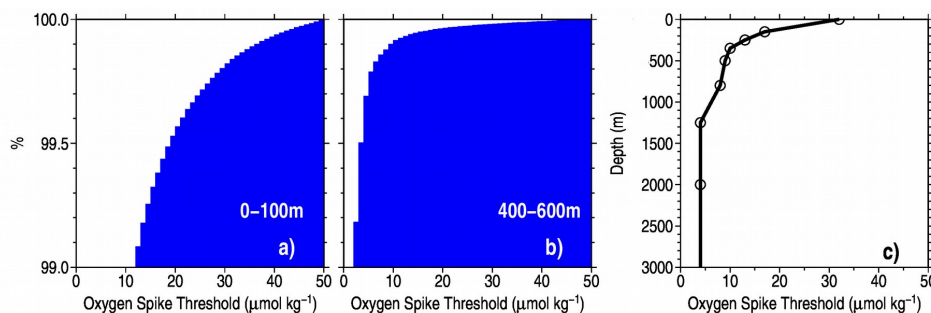


**Figure 8. Spike magnitude histograms for the layer 0-100m (a), 400-600m (b) and spike threshold values versus depth (c).**

215

216 **3.6 Multiple extrema check**

217 Multiple extrema check aims to identify profiles whose shape significantly deviates from majority of profiles. For each  
 218 profile with at least 5 observed levels (see schematics in Fig.9), the number of local extrema (black dots) and their  
 219 magnitudes (denoted as  $M_n$  in Fig.9) are calculated. Then frequency histograms of oxygen profiles for different  
 220 combinations of the number of oxygen extrema and of the extremum magnitude are calculated (**Fig. 10**). As can be  
 221 seen from the histograms the larger the extremum magnitude, the less frequent are the profiles with multiple extrema of  
 222 this magnitude. Grey areas of histograms correspond to the outlier profiles, e.g. profiles exhibiting too many local  
 223 extrema for a given extremum magnitude threshold value.



224

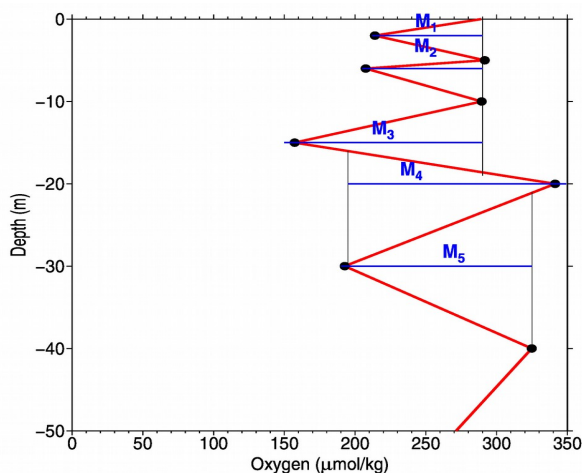


**Figure 9.** Schematics for the local extrema check. Black dots represent the local extrema ( $M$ ), whereas extremum magnitudes are shown with blue lines.

225

226 Normalized histograms showing the frequency of profiles as the function of the number of extrema and the extremum  
 227 magnitude value are given in Fig.10. Grey areas correspond to the outlier profiles, e.g. profiles exhibiting too many  
 228 local extrema for a given extremum magnitude threshold value. The histograms were produced for three  
 229 instrumentation types. The histogram for Argo profiles differs from those for OSD and CTD because it is based on  
 230 profiles that the respective DACs have already validated.

231

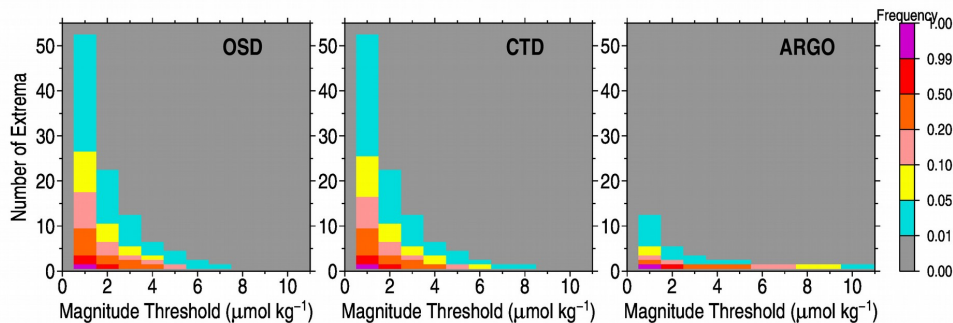


**Fig.10.** Normalized frequency histograms for multiple extrema check: a) OSD, b) CTD, c) Argo profiles. Grey areas correspond to the oxygen profiles failing the multiple extrema check.

232

### 233 3.7 Oxygen Vertical Gradient check

234 The oxygen vertical gradient check aims to identify pairs of levels for which the vertical oxygen gradient exceeds a  
 235 certain threshold. Threshold values (Fig. 11) are calculated for several layers to account for the change of gradient



236 values with depth. The thresholds are defined using six standard deviation envelopes around the mean gradient value.  
 237 Due to the nonlinearity of oxygen profiles, vertical gradient values depend on the profile's vertical resolution, e.g., from  
 238 the gap between two neighbor observed levels. Respectively, oxygen thresholds at each level are calculated for several  
 239 values of depth gaps, as Tan et al. (2023) did for the quality control of temperature profiles. Calculations are performed  
 240 separately for positive and negative oxygen gradient values. Because of a high oxygen vertical gradient variability in  
 241 the near-surface layer and over the entire World Ocean, we conduct vertical gradient check only for levels below 200 m  
 242 depth.  
 243

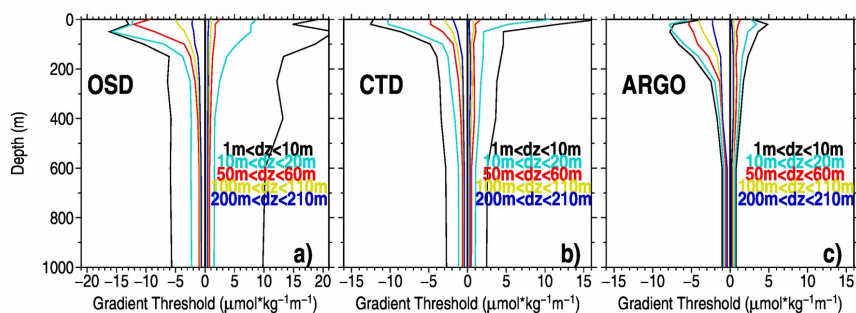


Figure 11. Oxygen vertical gradient threshold versus depth for several depth gaps ( $dz$ ) between the neighbor observed levels: a) OSD, b) CTD, c) Argo profiles.

### 244 3.8 Local Climatological range check

245 Local climatological oxygen range check is most effective for identifying outliers compared with other checks, because  
 246 the min/max thresholds constrain the observed values locally. For each  $1^\circ \times 1^\circ$  latitude/longitude grid point, we calculate  
 247 min/max thresholds taking into account the skewness of the data. For calculating climatological ranges, we assume the  
 248 ergodic hypothesis in which the average over time is considered to be equal to the average over the data ensemble  
 249 within a certain spatial influence radius. Taking into account the skewness of statistical distribution when defining  
 250 climatological ranges for oceanographic parameters was first suggested by Gouretski (2018), who applied Tukey's box  
 251 plot method modified for the case of skewed distributions (Hubert and Vandervieren, 2008; Adil and Irshad, 2015). In  
 252 this method lower ( $L_f$ ) and upper ( $L_u$ ) fences are calculated according to formula (1):

$$253 \quad [L_f \quad U_f] = [Q1 - 1.5 * IQR * \exp(-SK * |MC|) \quad Q3 + 1.5 * IQR * \exp(SK * |MC|)], \quad (1)$$

254 where  $Q1$ ,  $Q3$  are quartiles,  $Q2$  is sample median,  $SK$  is skewness.  $MC$  denotes medcouple, which is defined as  $MC =$   
 255 median  $h(x_i, x_j)$ , where  $x_i << Q2 << x_j$ ; and the kernel function  $h(x_i, x_j) = [(x_j - Q2) - (Q2 - x_i)] / (x_j - x_i)$ . (Hubert and  
 256 Vandervieren, 2008).  
 257  
 258  
 259

260 We note that the local oxygen thresholds are constructed using the data which have undergone the preliminary quality  
 261 control. This control includes checks for crude range, spikes, stucked value, and multiple extrema, and vertical  
 262 gradient, aiming to remove most outlying scores in order to reduce their impact on the local thresholds. This approach  
 263 is similar to the two-stage thresholding suggested by Yang et al. (2019).



264

265

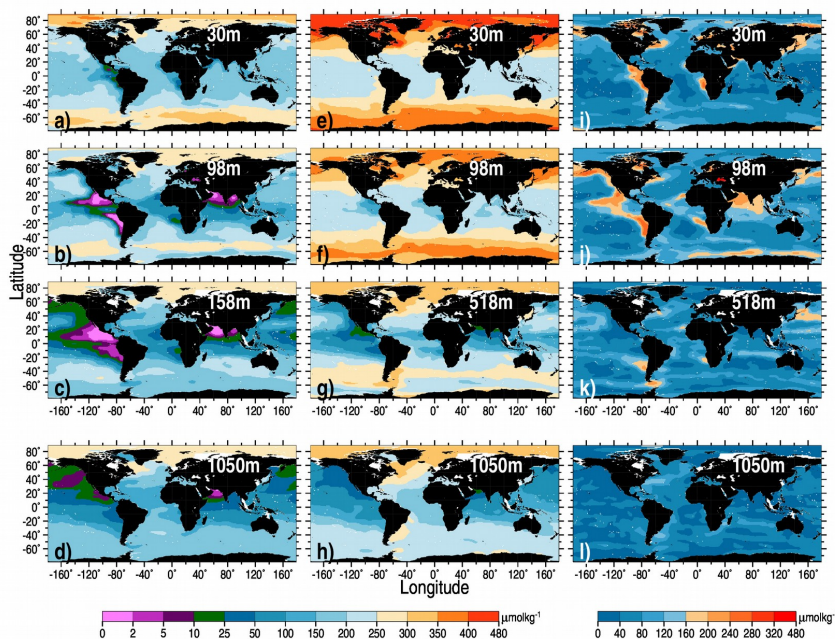


**Fig.12.** Local climatological lower oxygen threshold for several depth levels: 30m (a), 98 m (b), 158m (c), 1050m (d). (e-h): same but for the upper oxygen threshold; (i-l) same but for the local oxygen range.

266 OSD validated data were used to construct maps of local minimum and maximum values at a set of depth levels using  
267 formula (1) (Fig. 12). The most striking features are the areas with low minimum oxygen values (oxygen minimum  
268 zones, Fig. 12a-c) in the East Pacific, Arabian Sea, Bay of Bengal, Black Sea, and Baltic Sea. The maps reflect wide  
269 oxygen ranges (Fig. 12 i-l) in several regions of the world's oceans, especially in the East Pacific and the North Indian  
270 oceans. The maps also depict higher oxygen variability in the highly dynamic regions of Gulf Stream, Kuroshio, and in  
271 the upwelling areas west of Africa. During the quality control, gridded minimum and maximum local oxygen values are  
272 interpolated to the profile locations.

### 273 3.9 Excessive flagged level percentage check

274 After applying all distinct quality checks, the percentage of flagged levels for each oxygen profile is calculated. The  
275 respective histograms (Fig. 13) are used to set thresholds to decide on the quality of the entire profile. Using these  
276 histograms as guidance, we set 30%, 10%, and 30% thresholds for OSD, CTD, and Argo profiles, respectively. If the  
277 threshold is exceeded, the entire profile is flagged. Both the OSD and the Argo profiles are characterized by a low  
278 number of profiles with a high percentage of flagged data. The OSD and Argo groups are characterized by a low  
279 percentage of profiles with a high number of rejected levels. In contrast, in the CTD group, most not-dummy oxygen  
280 values fail quality checks, resulting in a high percentage of flagged profiles.

281

282

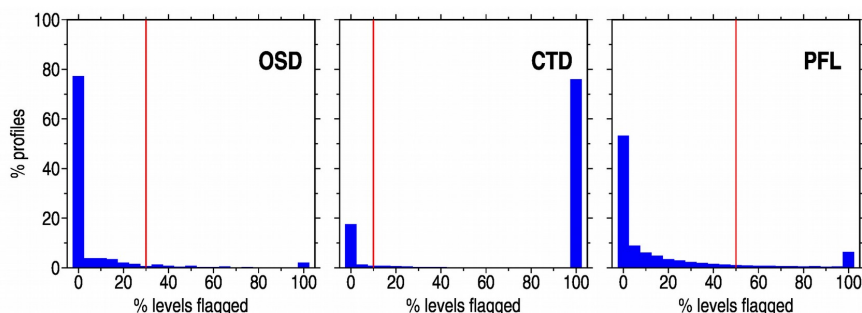


Fig.13. Percentage of oxygen profiles versus percentage of rejected levels per profile for OSD, CTD, and Argo instrument types.

283 **4 Oxygen Data Quality Assessment based on the results of the automated quality control procedure**

284 Table 1 and Fig. 14 summarize the rejection rates for all nine quality checks and the three instrumentation types  
 285 considered. The Argo oxygen profiles have the lowest overall rejection rate of 6.20%, with Winkler data quality (9.66%  
 286 outliers) ranking second best. We explain this difference through two factors. First, Winkler profiles cover a century-  
 287 long period of observations, with a worse data quality in the earlier decades. Secondly, the analyzed Argo oxygen data  
 288 are represented by adjusted profiles, which have been already quality-controlled.

289

290 The CTD oxygen profiles are characterized by the highest percentage of outliers. This is attributed to many high-  
 291 resolution CTD profiles reporting oxygen values, identified as outliers by multiple quality checks, and probably  
 292 representing the digital output of the malfunctioning oxygen sensors. The local climatological range check (No.8)  
 293 results in the highest percentage of flagged observations and the profiles affected by this check. In the case of OSD  
 294 profiles, about 18% of profiles have at least one flagged measurement. For Argo oxygen profiles, this percentage is  
 295 about 30%.

296

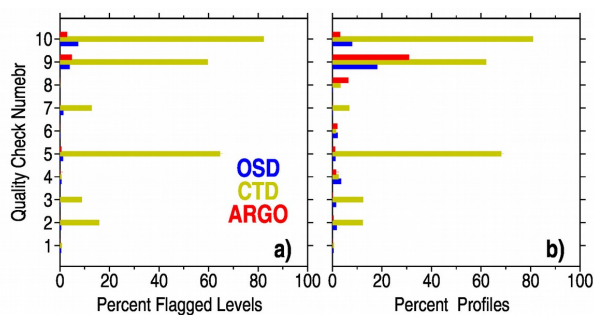


Figure14. Percentage of rejected observations for distinct quality checks and three instrumentation types: a) percent of flagged level; b) percent of profiles affected by the respective check. Check number is indicated in Table 2.

297

298

299



300

301

302

**Table 2 Outlier score statistics for different instrumentation types**

		OSD		CTD		ARGO	
	Quality Check	% flagged observations	% flagged profiles	% flagged observations.	% flagged profiles	% flagged observations	% flagged profiles
1	Location check	0.452	0.515	0.719	0.532	0.092	0.081
2	Global Oxygen Range at depth levels	0.414	1.772	15.797	14.246	0.041	0.420
	Global Oxygen Range on T surfaces	0.272	1.511	8.824	12.381	0.009	0.221
3	Supersaturation check	0.654	3.524	0.635	2.458	0.101	1.496
4	Stucked value check	1.265	1.168	64.596	68.086	0.564	1.060
5	Spike check	0.226	2.151	0.043	1.527	0.012	1.873
6	Multiple extrema check	1.376	0.233	12.846	6.801	0.126	0.057
7	Oxygen vertical gradient check	0.205	1.036	0.536	9.223	0.139	7.671
8	Local climatological range	3.922	18.151	59.663	62.013	4.824	30.915
9	Excessive flagged level percentage profile check	7.397	7.948	82.288	80.912	2.910	3.136
	ALL QC CHECKS	9.66	23.88	82.97	88.69	6.20	36.65

303

304 **5 Benchmarking of the automated quality control procedure using manually controlled datasets**

305 Good et al. (2022) conducted a comprehensive benchmarking exercise to evaluate the performance of AQC checks on  
 306 temperature profiles implemented by different research groups, aiming to recommend an optimal set of quality checks.  
 307 They used several reference datasets with known quality (e.g. evaluated by means of expert control). The procedure  
 308 does not include the assessment of temperature biases. This study uses a comprehensive set of bottle profile data  
 309 obtained during the World Ocean Circulation Experiment (WOCE) – the largest international oceanographic experiment  
 310 ever conducted (Wunsch, 2005). To achieve a high degree of data quality and consistency between the cruises over the  
 311 entire period of observations, the WOCE Hydrographic Program Office (WHPO) issued operation manuals (WHPO,  
 312 1991), where methods and procedures are described. As shown by Gouretski and Jancke (2000) the WHPO quality  
 313 requirements have been fulfilled with the WOCE hydrographic dataset representing a unique global scale collection of  
 314 the whole suite of oceanographic parameters. Specifically, the mean inter-cruise oxygen offset was found to be 2.389  
 315  $\mu\text{mol kg}^{-1}$ . After completing the WOCE, the GO-SHIP program was established in 2007 to revise the WOCE  
 316 hydrographic programme (Hood et al, 2010). Applying our quality control procedure to the entire WOCE dataset  
 317 confirms the high quality of this unique dataset, with only 2.85% of oxygen outliers (Fig. 15a, b) for the entire time  
 318 period 1990-1998. The QC diagnostics reflect the progressive improvement of the oxygen data quality over the period  
 319 of WOCE (Fig. 15a). Flagging rate as depicted on oxygen vs depth diagram (Fig. 15a) illustrates the ability of the QC  
 320 procedure to identify outliers deviating from the main population. The spatial distribution of outliers for the entire time  
 321 period (Fig. 15c) indicates the majority of WOCE oxygen profiles having a very low percentage of outliers or exhibiting



322 no outliers at all. The high percentage of oxygen outliers is found only for several WOCE lines in the tropical South  
323 Atlantic, North-Western Indian Ocean, and the Labrador Sea.  $\mu\text{mol kg}^{-1}$   
324 The WOD database permits data selection for a large number of observational programs using the respective  
325 project identification code. The outlier rejection percentage for the data from 128 projects that reported oxygen data is  
326 shown in Fig. 16. Several outstanding observational programs like GEOSECS (Geochemical Ocean Sections Study)  
327 (Craig, 1974), SAVE (South Atlantic Ventilation Experiment) (Larque et al., 1997), WOCE, CARINA (Carbon dioxide  
328 in the Atlantic Ocean) (Falck and Olsen, 2010), and CLIVAR (Climate and Ocean: Variability, Predictability and  
329 Change) (Sarachick, 1995) delivered a significant number of high-quality data. We note that the four projects with a  
330 median year after 1985 (SAVE, WOCE, CARINA, and CLIVAR) are characterized by the rejection rates lower than the  
331 mean. For instance, for the largest WOCE dataset the QC procedure identifies only 2.8% from the total of 354028  
332 oxygen measurements (Fig. 16a) with 79% percent of oxygen profiles without data outliers (Fig. 16b).

333

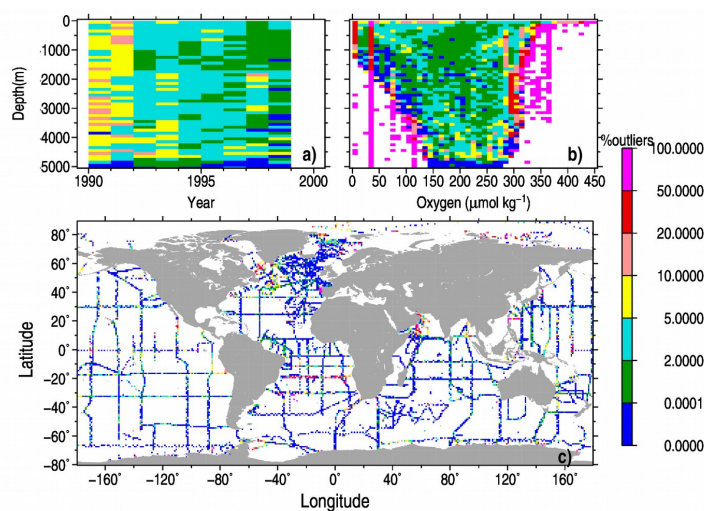


**Figure 15.** Quality control statistics for WOCE dataset: a) percentage of outliers in year/depth bins; b) percentage of outliers in oxygen/depth bins; percentage of outliers in 1x1-degree squares.

## 334 6 Bias assessment for sensor oxygen data

335 The quality control procedure described in the previous sections is based on the underlying statistics of the data and  
336 aims to identify random outliers. The second step in data quality control is estimating the possible systematic errors or  
337 biases. These systematic errors may differ depending on the instrumentation type, but the common fcause for systematic  
338 errors is the absence of the possibility to calibrate the instrument. A classic example provides temperature data obtained  
339 by eXpandable bathythermographs (XBT) where systematic errors are due to the uncertainty in depth, which is  
340 calculated from the elapsed time, and the uncertainty in thermistor, which is typically not calibrated (Gouretski and  
341 Reseghetti, 2010; Cheng et al. 2014). In the case of dissolved oxygen, only Winkler measurements of discrete samples  
342 can be considered to be bias-free because the chemical analysis is based on the  $\text{KIO}_3$  standard reference, with the  
343 replicate measurements having a precision better than  $0.4 \mu\text{mol kg}^{-1}$  (Thaillandier et al., 2018). In the following, we  
344 describe residual biases for CTD and Argo profiles. The term “residual” is used because CTD oxygen profiles are



345 typically adjusted on Winkler bottle samples, and Argo oxygen profiles used in our study undergo adjustment  
346 procedures at the respective DACs.

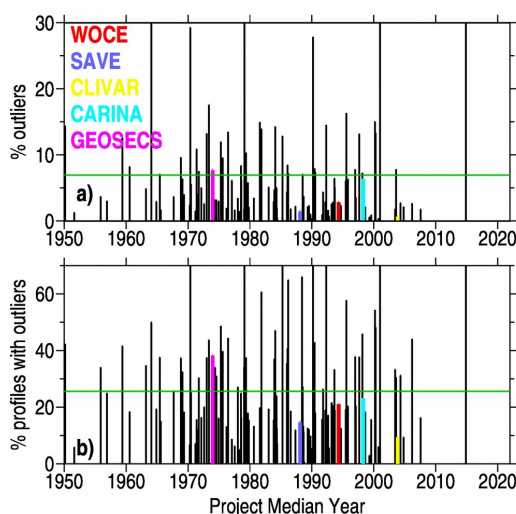


**Figure 16. Outlier diagnostics for 128 distinct WOD projects (OSD Winkler profiles). a) Overall percent of outliers; b) percent of profiles with oxygen outliers. Acronyms and percentages for selected hydrographic projects described in text are shown in color.**

347 Use of electrochemical and optical oxygen sensors into oceanographic practice has two main aspects. First,  
348 these sensors permitted a significantly higher rate of data acquisition and a much finer vertical resolution than bottle  
349 data. Secondly, they made the observational process much easier than bottle samples, which need chemical titration in  
350 the laboratory. However, like other electronic sensors, oxygen sensors are prone to offsets and drift. Takeshita et al  
351 (2013) analyzed data from 130 Argo floats and found a mean bias of -5.0 % O<sub>2</sub> saturation at 100 % O<sub>2</sub> saturation. Bittig  
352 et al (2018) explained this negative bias by reducing O<sub>2</sub> sensitivity proportional to oxygen content, with the decrease of  
353 sensitivity being on the order of several percent per year. Optode drift characteristics require regular calibration. Use of  
354 reference Winkler profiles is possible only for the ship-based CTD oxygen sensors (mostly electrochemical sensors) if  
355 CTD rosette water samples are obtained simultaneously with sensor profiles and are analyzed for oxygen during a  
356 cruise (Uchida et al., 2010). For unmanned autonomous platforms like Argo, the direct comparison with reference  
357 Winkler data is limited to samples from the hydrographic casts conducted during the float deployment. Bittig et al.  
358 (2018) recommended adjusting optode data on oxygen partial pressure primarily by the gain (Argo Quality Control  
359 Manual, 2021). If no previous delayed-mode adjustment is available, the basic real-time adjustments are performed





360 based on the oxygen saturation maps provided by the WOA digital climatological atlas (Thierry et al., 2021). In case a  
361 delayed-mode adjustment is not available after one year, the re-assessment of the gain factor is recommended.  
362 Uncertainty in underlying optode calibration and time drift characteristics leads to errors in adjusted data.

### 363 6.1 Bias assessment method

364 We aim to assess the magnitude of the possible overall residual bias for CTD profiles and adjusted Argo optode profiles  
365 by comparing these profiles with collocated reference discrete samples. The data from 10 national DACs were used for  
366 this analysis, for which both unadjusted and adjusted oxygen profiles are available. Data centers and the respective  
367 number of oxygen profiles are given in Table 2. We use the Winkler method oxygen profiles available from the World  
368 Ocean Database and described in Section 1.1. These profiles are used as reference data for the comparison with  
369 collocated Argo optode oxygen profiles.

370

371 For the current analysis, we selected a 100 km threshold distance within which two profiles are spatially collocated. To  
372 decide upon the choice of the optimal maximum time difference between Argo and reference profiles, we calculated  
373 median oxygen offsets increasing threshold value for the time separation between a pair of profiles (Fig.17a). Increasing  
374 the temporal collocation bubble leads to the increase of the bias magnitude in agreement with the assumption that the  
375 older reference data are richer in oxygen compared to the more recent data. Below 1000 m depth, the difference  
376 between the median offsets for the temporal collocation bubble of 5 and 50 years is about  $3.5 \mu\text{mol kg}^{-1}$ , corresponding  
377 to a deoxygenation trend of about  $0.7 \mu\text{mol kg}^{-1}$  per decade. This estimate can be compared with  $0.75 \mu\text{mol kg}^{-1}$  per  
378 decadedec reported by Gregoire et al. (2021). As Fig. 17c suggests, the overall offset estimate below 1000 m stabilizes  
379 after the time difference threshold of 5 years. The extension of the temporal bubble for more than 7 years leads to the  
380 progressive increase of the bias magnitude, which we attribute to the impact of the general deoxygenation. Based on  
381 these calculations, the 5-year threshold was selected as the maximum time separation between collocated profiles. For  
382 this threshold value, the number of collocated pairs below 1000m depth is about 10000 (Fig. 17b). A step-wise decrease  
383 of the number of collocated pairs below 950 m is explained by a significant part of reference profiles being limited to  
384 the upper 1000-meter layer. These calculations suggest that about 1000 collocated pairs are required for stable offset  
385 estimates.

386

387

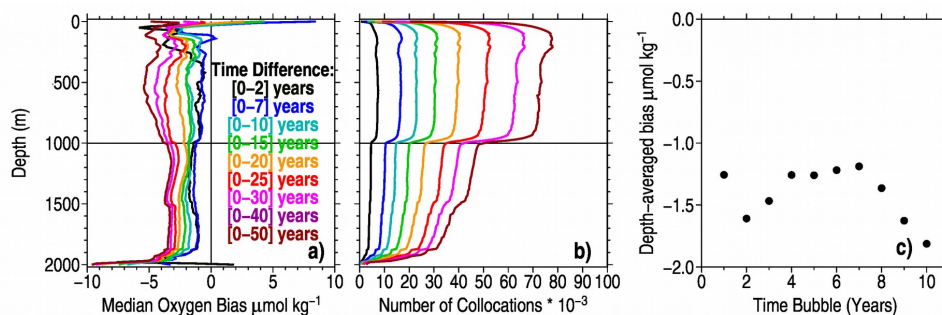


Figure17. a) Overall median oxygen bias versus the size of the temporal collocation bubble; b) number of collocated pairs for different choices of collocation bubbles; c) depth-averaged (1000-1900m) bias versus time bubble size.

388



389 The number of Argo profiles having collocations with discrete ship-based Winkler profiles is shown in Table 2. No  
390 collocated Winkler profiles are found for the Argo profiles from the two Korean DACs. Profiles from these DACs are  
391 restricted within a relatively small area east of the Korean peninsula. The four largest contributors of Argo data (AOML,  
392 Coriolis, JMA, and CSIRO) comprise up to XX percent of all Argo profiles having collocations with reference profiles

## 393 6.2 Overall bias characteristics

394 The normalized frequency histograms (Fig. 18) characterize the spread of individual bias estimates around the  
395 distribution mode. These histograms are based on all Argo profiles having collocations with reference Winkler data. In  
396 these histograms, for each depth bin, the number of values in each bias bin is normalized by the number for the most  
397 populated bias bin. The adjustment procedures applied in different DACs reduce the spread of the individual bias  
398 estimates and significantly reduce the overall median bias from 10-12  $\mu\text{mol kg}^{-1}$  for unadjusted data to 1-2  $\mu\text{mol kg}^{-1}$  for  
399 adjusted data. Based on the histogram, we estimate residual bias using the collocated data below 1000 m depth, where  
400 the natural variability is reduced compared to the upper part of the water column.

401  
402

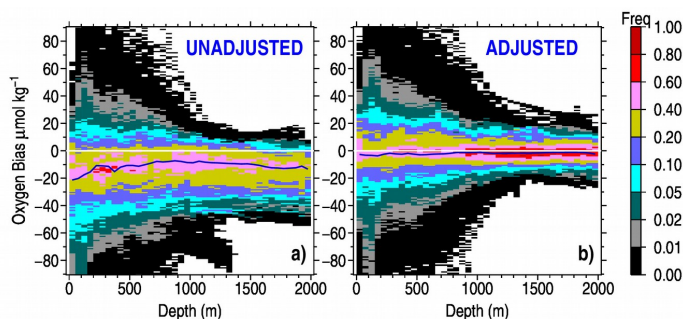


Fig.18. Normalized histograms of the unadjusted (a) and adjusted (b) Argo oxygen offsets versus collocated Winkler profiles. The blue curve shows the median.

403

## 404 6.3 Residual Oxygen Biases for Argo profiles from distinct DACs

405 According to the Argo Quality Control Manual (Thierry et al., 2021), several adjustment procedures can be applied to  
406 unadjusted data (adjustment to climatology, adjustment to nearby Winkler samples, adjustment to in-air data). The  
407 adjustment results may depend on many factors, such as the subjective decision of the operator in a DAC, the use of a  
408 specific software, the availability of the respective reference data, etc.). If a climatology is used as a reference, the  
409 adjusted Argo oxygen values will be adjusted to the median year of a climatology, which can differ by several decades  
410 from the year of an Argo profile. In such cases, the long-term deoxygenation trend of the world ocean might bias the  
411 results of the adjustment procedure.

412 Changes in oxygen sensors over time may cause respective changes in diagnosed biases. Fig. 19 shows the  
413 yearly number of observed profiles of AOML-processed Argo floats equipped with different models of optode sensors.  
414 Since the beginning of the 2000s, several different models of optodes were implemented in BGC Argo floats, with the  
415 most widespread sensors being AANDERAA 3830, implemented between 2004 and 2018, and the following model  
416 AANDERAA 4330. Since about 2013, the majority of Argo floats from the two largest AOML and Coriolis datasets



417 have been equipped with this sensor. The AANDERAA 4330 sensor prevails between 2012-2017 for JMA data and after  
418 2020 for CSIRO data (Fig. 19.)  
419  
420  
421  
422

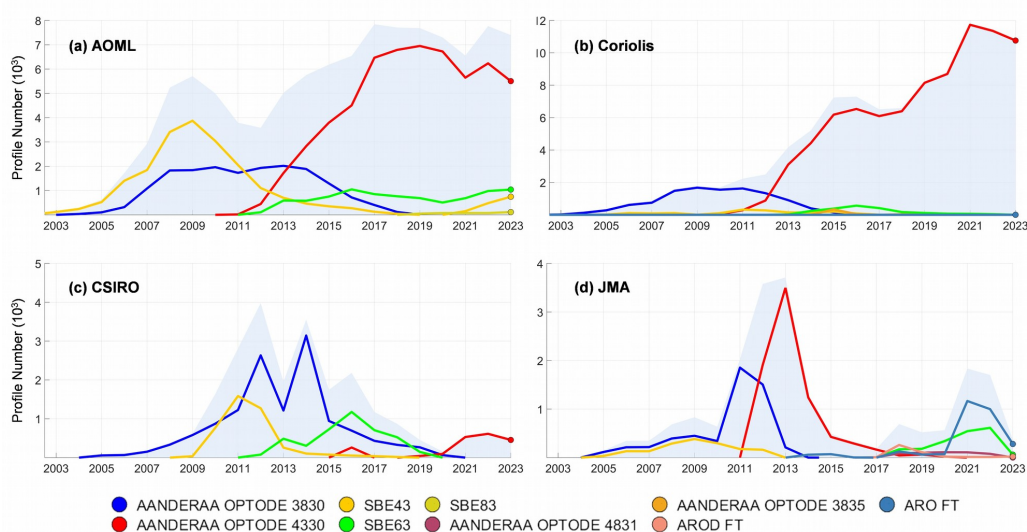


**Figure 19. Yearly number of BGC Argo profiles equipped with different types of optode oxygen sensors (colored lines). Light-blue shading corresponds to the total number of profiles: a) AOML, b) Coriolis, c) JMA, d) CSIRO**

423 We calculated the residual oxygen bias for each depth level as the mean offset between Argo and Winkler  
424 oxygen data over all collocated pairs for each DAC (Fig. 20). The offsets for the Korean DACs cannot be estimated  
425 due to the lack of the collocated Winkler profiles. The number of available collocations with reference Winkler profiles  
426 varies by the order of magnitude for different DACs. Since reference bottle data often cover only part of the upper  
427 2000-meter layer, the number of collocated pairs also changes over depth, with the main step-wise decrease seen around  
428 1000m. A comparison of the vertical bias profiles for other DACs suggests that changes in the number of collocated  
429 pairs over depth do not impact the diagnosed bias. Except for CSIRO and MEDS Argo profiles, DAC-adjusted overall  
430 median residual bias is negative, ranging between -1.0 to -3.6  $\mu\text{mol kg}^{-1}$ . The residual positive bias for CSIRO and  
431 MEDS profiles is typically within the range of 0.4-0.6  $\mu\text{mol kg}^{-1}$  below 1000 m. INCOIS profiles are characterized by  
432 the change from negative to positive bias below 1400 m.

433 For the two largest datasets (e.g., AOML and CORIOLIS), vertical bias profiles exhibit a characteristic hook  
434 below about 1900-1950 meters. Such hooks on Argo oxygen profiles were found by (Thallander et al., 2018). The hook  
435 can reflect the adjustment of the oxygen sensor at the beginning of the float ascending.

436 To investigate a possible bias change over time due to the change in the instrumentation (see Fig. 19), we first  
437 calculated depth-averaged biases (1000-1900m layer) for each collocation pair. Mean biases within  $2^\circ \times 4^\circ$  latitude-  
438 longitude boxes are shown in Fig. 21, along with the bias histograms for two time periods: 2005-2013 and 2014-2023.



439 The choice of these two periods approximately corresponds to the instrumentation change around 2013, which was  
 440 described above. The calculations were done separately for each DAC. During the first period, the foil-batch calibrated  
 441 optodes were used predominantly. Bittig et al. (2018) note that differences between batch calibration and individual  
 442 optode can exist. For the MEDS dataset, only data from the period 2004-2013 are available. For the largest AOML  
 443 dataset, the 2014-2023 period is characterized by a stronger negative bias of  $-3.54 \mu\text{mol kg}^{-1}$  compared to  $-0.25 \mu\text{mol}$   
 444  $\text{kg}^{-1}$  for the time period 2004-2013 (Fig. 20a). We explain this AOML residual bias change by the respective  
 445 instrumentation change (Fig. 19). However the second largest Coriolis dataset does not show a significant difference  
 446 between these time periods (Fig. 20b), what could reflect differences in the adjustment procedures implemented by  
 447 AOML and Coriolis DACs.  
 448  
 449

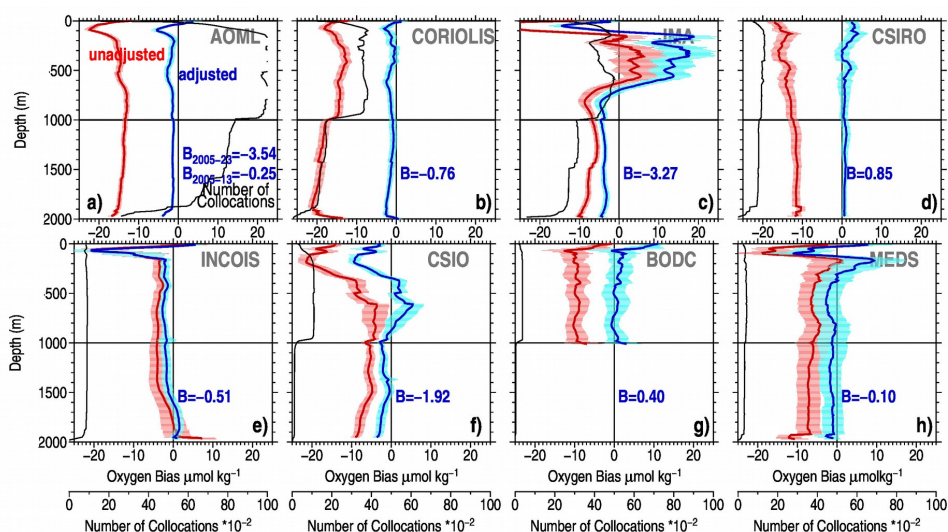


**Figure 20.** Overall mean Argo oxygen offsets vs Winkler profiles for distinct DACs: a) AOML, b) Coriolis, c) JMA, d) CSIRO, e) INCOIS, f) CSIO, g) BODC, h) MEDS. Offset profiles for unadjusted and adjusted data are shown in red and blue, respectively. Standard error bars (light shading) are calculated using the number of different floats at each level as the number of degrees of freedom. Blue numbers show the depth-averaged residual offsets ( $\mu\text{mol kg}^{-1}$ ) within the layer 1000-1900m. Black thin lines show the number of collocated pairs at depth levels.

450

451

#### 452 6.4 Residual Oxygen Biases for distinct Argo floats

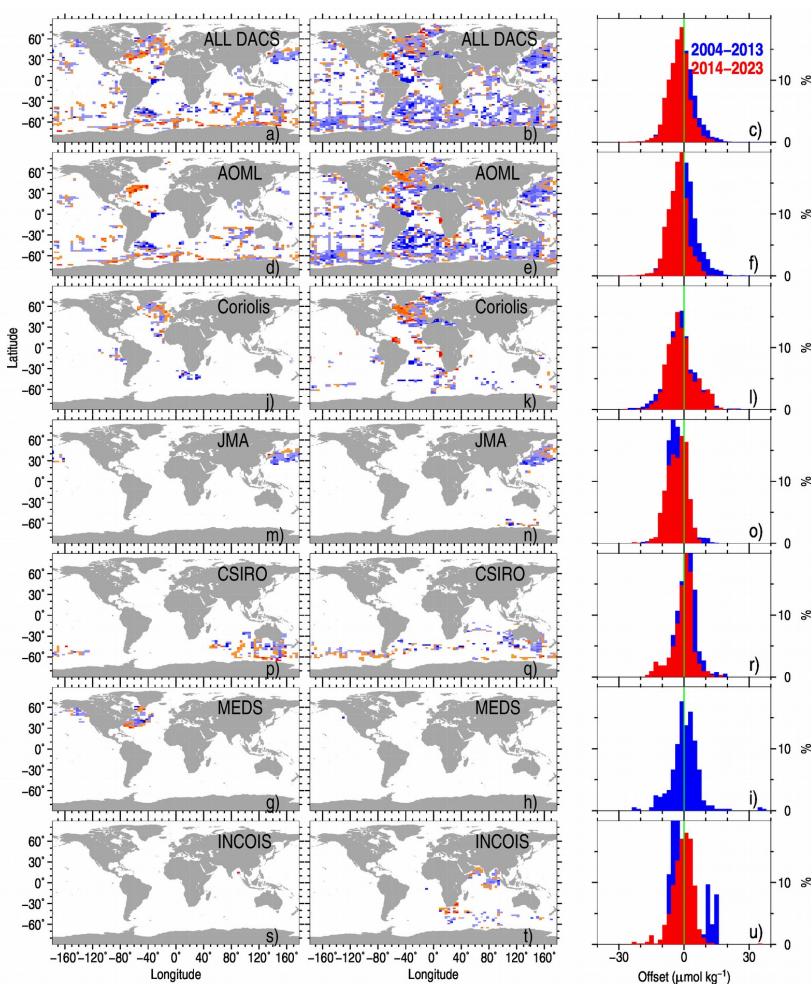
453 In addition to the overall biases described above, we also calculated biases for distinct Argo floats (Fig.22). The scatter  
 454 diagrams of adjusted versus not-adjusted data show that the overwhelming majority of floats exhibit adjusted residual  
 455 biases of a smaller magnitude compared to unadjusted data. Among 1020 Argo floats for which at least ten profiles with  
 456 individual profile offsets between 1000 and 1900m are available, oxygen adjustments for 22 floats (3.1%) were found to  
 457 be unsuccessful. However, the magnitude of most of these misfits does not exceed  $2 \mu\text{mol kg}^{-1}$  and is well within the  
 458 uncertainty of bias estimation for individual floats.

459



460 **6.5 Residual Oxygen Biases for CTD oxygen sensors**

461 We conducted similar bias calculations for the WOD CTD oxygen profiles, mostly obtained by electrochemical sensors.  
 462 Unlike Argo profiles, the CTD oxygen sensor data are typically adjusted on the simultaneously obtained bottle samples  
 463 analyzed in the ship laboratory using the Winkler method (Thaillandier et al., 2018). Therefore the overall mean CTD  
 464 residual bias is small compared to the residual Argo oxygen bias. Within the layer 1000-1900m, CTD oxygen bias is in  
 465 the range of 0.2-0.5  $\mu\text{mol kg}^{-1}$ , with the mean value close to 0.3  $\mu\text{mol kg}^{-1}$  (Fig.23). Above the 1000 m level the bias  
 466 exhibits stronger variability which we explain by the impact of the increased spatial and temporal variability above the  
 467 main thermocline.  
 468



469 **Figure 21. Residual oxygen bias in  $2^{\circ}\times 4^{\circ}$  boxes for DAC-adjusted oxygen values for all collocated pairs: a) years 2004-2013;**  
 470 **b) years 2014-2023; c) bias histograms for two periods. d-f) same for AOML data; g-i) same for MEDS data; j-l) same for**  
 471 **Coriolis data; m-o) same for JMA data; p-r) same for CSIRO data; s-u) same for INCOIS data.**  
 472



473

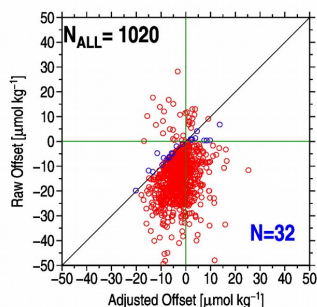


Figure 22. Raw versus adjusted oxygen bias for distinct BGC Argo floats (layer 1000–1900 m). Bad adjustments are shown in blue.

474

475

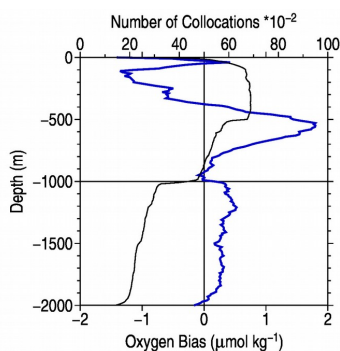


Figure 23. Overall mean oxygen offset CTD-Winkler (blue) and the number of collocated pairs (black)

476

## 477 8 Summary and Conclusions

478 This study developed a new automated quality control scheme for ocean oxygen profile data and applied it to the  
479 oxygen profiles from the World Ocean Database and the Argo float oxygen profiles provided by national DACs. The  
480 procedure consists of a suite of nine quality checks, which are based on local or global parameter thresholds. Some  
481 checks are conceptually similar to the quality checks used to validate the profiles in the World Ocean Database (Boyer  
482 et al., 2018) (for example, global range test, vertical gradient test) and in the Argo data acquisition centers (Thierry et  
483 al., 2021) (for example, spike, frozen profile tests), but we provide additional checks (for example, test for the number  
484 of local extrema and local climatological range test) which have several advantages to better flag likely erroneous data.  
485 For instance, the procedure proves whether an oxygen value falls out of accepted ranges (defined by global or local  
486 ranges) or whether an oxygen profile exhibits a very untypical shape. The shape of the profile is characterized by the  
487 vertical oxygen gradient, the number and magnitude of local oxygen extrema, and the presence of spikes. The check is  
488 also done for the so-called “frozen” profiles occurring when the oxygen sensor stocks and reports the same values  
489 throughout the profile.



490 The novelty of the proposed quality scheme is that the threshold choice is based on the respective statistics,  
491 and the Gaussian distribution is not assumed for the local climatological range check. The accompanying diagnostic  
492 tool provides the overview of outlier scores and permits tuning the thresholds. The quality control procedure was  
493 benchmarked against several hydrographic datasets known for their outstanding measurement quality, with WOCE  
494 experiment data collection being the largest and best documented. Analysis of the outliers and their distribution among  
495 distinct hydrographic sections suggests the ability of the procedure to flag outliers retaining the overwhelming majority  
496 of good data.

497 Further, we estimated possible residual oxygen biases in the delayed-mode adjusted Argo oxygen profiles. The  
498 bias estimates are based on analyzing the collocated Argo and discrete water sample ship-based profiles. The latter  
499 represents reference measurements as the bottle samples are analyzed by means of the Winkler chemical method. The  
500 size of the collocation bubble (e.g., the maximum distance between two profiles and the maximum time difference)  
501 have been set by 100 km and 5 years, respectively, after conducting several experiments for different bubble sizes.  
502 Residual biases relative to the Winkler reference data are represented by the difference at an isobaric level between the  
503 Argo sensor oxygen value and the Winkler oxygen, with the overall residual bias at each level being defined by the  
504 average overall individual differences.

505 Our calculations find a small negative residual oxygen bias in the range  $-1$  to  $-4 \mu\text{mol kg}^{-1}$  for all individual  
506 DAC datasets except CSIRO and MEDS. The residual positive bias for CSIRO and MEDS profiles is typically within  
507 the range of  $0.5$ - $1.0 \mu\text{mol kg}^{-1}$  below 1000 m. Calculations suggest at least an order of 1000 collocations is needed for  
508 the stable residual bias estimation. This number of collocations is available only for AOML, Coriolis, JMA, CSIRO,  
509 and INCOIS datasets. Further, we found a change in the diagnosed residual oxygen bias around 2014 for the largest  
510 AOML dataset, possibly related to the instrumentation change, when the AANDERAA optode A4330 became the  
511 primary sensor type used on Argo floats. However, this change of the residual bias could not be diagnosed for the  
512 second largest Coriolis dataset. Analysis of the residual bias for 1020 Argo floats having at least ten profiles with  
513 collocations confirmed bias reduction for 97% of the floats (compared to the unadjusted data) due to the adjustments  
514 conducted by DACs .

515 Diagnosed residual biases for the quality-controlled CTD oxygen sensor profiles revealed a high degree of  
516 agreement between the CTD and Winkler reference data, with the bias being in the range  $0.2$ - $0.5 \mu\text{mol kg}^{-1}$ . We explain  
517 this low bias as the result of the adjustment of CTD oxygen sensor data on simultaneous discrete samples analyzed by  
518 the Winkler method.

519 In summary, this study proposed a new QC approach to process CTD, bottle, and Argo data and investigated  
520 the consistency between the three primary instrumental data for ocean oxygen. Our investigations ensure the  
521 consistency between the three datasets and provide a solid basis for merging the three datasets into a single, integrated,  
522 and homogeneous oxygen database. Therefore, the database obtained in this study supports next-step assessment and  
523 understanding of the change in ocean oxygen levels.

524

525

## 526 7 Data availability

527

528 The quality control procedure described above was applied to the OSD and CTD oxygen profiles between 1920 and  
529 2023 from the World Ocean Database and to the oxygen profiles from the BGC Argo floats. The resulting dataset



530 comprises observed level data with quality flags and data interpolated on 10-meter levels. The data are in NetCDF  
531 format and also include the metadata information. The complete dataset (Gouretski et al., 2023) can be found at  
532 <http://dx.doi.org/10.12157/IOCAS.20231208.001>.

#### 533 **Author contributions.**

534 LC and VG – conceptualization, supervision, methodology; VG – software, formal analysis, data validation,  
535 visualization, and writing (original draft preparation, final version, and editing); JD., XX, FC – methodology, data  
536 curation; LC –funding acquisition.

537

538 **Competing interests.** The contact author has declared that none of the authors has any competing interests.

539

540 **Acknowledgements.** We are thankful to the institutions and organizations that provided the data used in this paper (the  
541 specific datasets and sources are as described in the text). We also thank all anonymous reviewers for their detailed and  
542 constructive comments. The Argo data were collected and made freely available by the International Argo Program and  
543 the national programs that contribute to it (ARGO, 2000). The Argo Program is part of the Global Ocean Observing  
544 System.

545

546 **Financial support.** This study was supported by the Strategic Priority Research Program of the Chinese Academy of  
547 Sciences [grant number XDB42040402], the National Natural Science Foundation of China [grant numbers 42122046  
548 and 42076202], and the Youth Innovation Promotion Association, CAS [grant number 2020-077]. The author also  
549 acknowledges the support from the new Cornerstone Science Foundation through the XPLOER PRIZE, Youth  
550 Innovation Promotion Association, Chinese Academy of Sciences.

551

#### 552 **References**

- 553 Adil, I. H. and Irshad, A. R.:A modified approach for detection of outliers, *Pak. J. Stat. Oper. Res.*, XI, 1, 91-102.  
554 Argo (2000). Argo float data and metadata from Global Data Assembly Centre (Argo GDAC).  
555 SEANOE. <https://doi.org/10.17882/42182>
- 556 Bittig, H. C., Maurer, T.L., Plant, J. N., Schmechtig, C., Wong, A. P. S., Claustre, H., Trull, T. W., Udaya Bhaskar, T. V.  
557 S., Boss, E., Dall’Olmo, G., Organelli, E., Poteau, A., Johnson, K. S., Hanstein, Leymarie, C., E., Le Reste, S.,  
558 Riser, S. C., Rupan, A., Taillandier, V., Thierry, V. and Xing, X. : A BGC-Argo Guide: Planning, Deployment,  
559 Data Handling and Usage, *Front. Mar. Sci.*, 6:502, doi: 10.3389/fmars.2019.00502, 2018.
- 560 Boyer, T. P., Baranova, O.K., Coleman, C., Garcia, H. E., Grodsky, A., Locarnini, R. A., Mishonov, A. V., Paver, C.  
561 R., Reagan, J. R., Seidov, D., Smolyar, I. V., Weathers, K., Zweng, M.M.: World Ocean Database 2018, A. V.  
562 Mishonov, Technical Editor, NOAA Atlas NESDIS 87, 2018.
- 563 Carpenter, J.H. :The accuracy of the Winkler method for dissolved oxygen analysis, *Limnology and*  
564 *Oceanography*, 10, 1, p. 135-140. <https://doi.org/10.3419/lo.1965.10.1.0135>, 1965.
- 565 Cheng, L. J., Zhu, J., Cowley, R., Boyer, T. and Wijffels, S.: Time, probe type and temperature variable bias corrections  
566 to historical expendable bathythermograph observations, *J. Atmos. Ocean. Technol.*, 31, 1793–1825,  
567 doi:10.1175/JTECH-D-13-00197.1, 2014.





- 568 Clark, L. C.: Cellophane/Platinum electrode for blood PO<sub>2</sub>, *J. Appl. Physiology*, 6, 189, 1953.
- 569 Claustre, H., Johnson, K. S., and Takeshita, Y.: Observing the global ocean with biogeochemical-Argo, *Annual*  
570 *Review of Marine Science*, 12, 23–48, 2020.
- 571 Coppola, L., Salvetat, F., Delauney, L., Machoczek, D., Larstensen, J., Sparnocchia, S., Thierry, V., Hydes, D., Haller,  
572 M., Nair, R., Lefevre, D.: White paper on dissolved oxygen measurements: scientific needs and sensors  
573 accuracy, 22 pages, 2013.
- 574 Cowley, R., Killick, R. E., Boyer, T., Gouretski, V., Reseghetti, F., Kizu, S., Palmer, M. D., Cheng, L., Storto, A., Le  
575 Menn, M., Simoncelli, S., Macdonald, A. M., and Domingues, C. M.: International Quality-Controlled Ocean  
576 Database (IQuOD) v0.1: The Temperature Uncertainty Specification, *Front. Mar. Sci.* 8:689695. doi:  
577 10.3389/fmars.2021.6896, 2021
- 578 Craig, H.: The GEOSECS program: 1972-1973: *Earth Planetary Science Letters*, v 23, p 63–64., 1974
- 579 Falck, E. and Olsen, A.: Nordic Seas dissolved oxygen data in CARINA, *Earth Syst. Sci. Data*, 2, 123–131, [https://](https://doi.org/10.5194/essd-2-123-2010)  
580 [doi.org/10.5194/essd-2-123-2010](https://doi.org/10.5194/essd-2-123-2010), 2010.
- 581 Garcia, H. E., Weathers, K., Paver, C. R., Smolyar, I., Boyer, T. P., Locarnini, R. A., Zweng, M. M., Mishonov, A. V.,  
582 Baranova, O. K., Seidov, D., and Reagan, J. R.: *World Ocean Atlas 2018, Volume 3: Dissolved Oxygen,*  
583 *Apparent Oxygen Utilization, and Oxygen Saturation.* A. Mishonov Technical Ed.; NOAA Atlas NESDIS 83,  
584 38pp, 2018.
- 585 Good., S., Mills, B., Boyer T., Bringas, F., Castelão, G., Cowley, R., Goni, G., Gouretski, V. and Domingues, C. M.:  
586 Benchmarking of automatic quality control checks for ocean temperature profiles and recommendations for  
587 optimal sets, *Front. Mar. Sci.*, DOI 10.3389/fmars.2022.1075510, 2022.
- 588 Gouretski, V., Cheng, L., Du, J., Xing, X., Chai, F.: A quality-controlled and bias-adjusted global ocean oxygen profile  
589 dataset, Marine Science Data Center of the Chinese Academy of Sciences,  
590 <http://dx.doi.org/10.12157/IOCAS.20231208.001>
- 591 Gouretski, V.: World Ocean Circulation Experiment – Argo Global Hydrographic Climatology, *Ocean Sci.*, 14,  
592 1127-1146, <https://doi.org/10.5194/os-14-1127-2018>, 2018.
- 593 Gouretski, V. and Reseghetti, F.: On depth and temperature biases in bathythermograph data: development of a  
594 new correction scheme based on analysis of a global database, *Deep-Sea Res.*, I, 57, 812-833, 2010.
- 595 Gouretski, V. V., and Jancke, K.: Systematic errors as the cause for an apparent deep water property variability:  
596 global analysis of the WOCE and historical hydrographic data., *Prog. Oceanogr.*, 48, 4, 337-402, 2000.
- 597 Gregoire, M. et al.: A Global Ocean Oxygen Database and Atlas for Assessing and Predicting Deoxygenation and  
598 Ocean Health in the Open and Coastal Ocean, *Front. Mar. Sci.*, 8, 1-29,  
599 <https://doi.org/10.3389/fmars.2021.724913>, 2021.
- 600 Hood, E.M., Sabine, C.L., and M. Sloyan, B.M., eds.: *The GO-SHIP Repeat Hydrography Manual: A Collection of*  
601 *Expert Reports and Guidelines*, IPCC Report Number 14, ICPO Publication Series Number 134, 2010.
- 602 Hubert, M. and Vandervieren, E.: An Adjusted boxplot for skewed distributions, *Comput. Stat. Data Anal.*, 52, 5186–  
603 5201, 2008.
- 604 Keeling, R.F., Koetzinger, A., and Gruber, N.: Ocean Deoxygenation in a Warming world, *Annu. Rev. Mar. Sci.*, 2,  
605 199-229. doi:10.1146/annurev.marine.010908.163855, 2010.



- 606 Koertzing, A., Schimanski, J., and Send, U.: High quality oxygen measurements from profiling floats: A promising  
607 new technique, *J. Atmos. Ocean. Technol.*, 22, 302-308, 2005.
- 608 Langdon, C.: Determination of Dissolved Oxygen in Seawater By Winkler Titration using Amperometric Technique,  
609 The GO-SHIP Repeat Hydrography Manual: A Collection of Expert Reports and Guidelines, Version 1, (eds  
610 Hood, E.M., C.L. Sabine, and B.M. Sloyan), 18pp.. (IOCCP Report Number 14; ICPO Publication Series  
611 Number 134), DOI: <https://doi.org/10.25607/OBP-1350>, 2010.
- 612 Larqué, L., Maamaatuaiahutapu, K., Garçon, V.: On the intermediate and deep water flows in the South Atlantic  
613 Ocean. *Journal of Geophysical Research*, 102,C6, <https://doi.org/10.1029/97JC00629>, 1997.
- 614 Marks, R.: Dissolved oxygen supersaturation and its impact on bubble formation in the southern Baltic Sea,  
615 *Hydrol. Res.*, 39,3, 229-236, 2008. Monhor, D. and Takemoto, S.: Understanding the concept of outlier and its  
616 relevance to the assessment of data quality: Probabilistic background theory, *Earth Planets Space*, 57, 1009–  
617 1018, 2005.
- 618 Sarachik, E.S.: CLIVAR: A Study of Climate Variability and Predictability: Science Plan. World Climate Research  
619 Programme Report 89, WMO Technical Document No 690. 157 pp, 1995.
- 620 Taillander, V., Wagener, T., D'Ortenzio, F., Mayot, N., Legoff, Ras, H. J., Coppola, L., De Fommervault, O. P.,  
621 Schmechtig, C., Diamond, E., Bittig, H., Lefevre, D., Leymarie, E., Poteau, A., and Prieur A.:  
622 Hydrography and biogeochemistry dedicated to the Mediterranean BGC-Argo network during a cruise with RV  
623 Tethys 2 in May 2015, *Earth Syst. Sci. Data*, 10, 627-641, 2018, <https://doi.org/10.5194/essd-10-627-2018>,  
624 2018.
- 625 Takeshita, Y., Martz, O. P., Johnson, K. S., Plant, J. N., Gilbert, D., Riser, S. C., Neil, C., and Tilbrook, B.: A  
626 climatology-based quality control procedure for plotting float oxygen data, *J. Geoph. Res: Oceans*, 118, 1-11,  
627 doi:10.1002/jgr.20399, 2013.
- 628 Tan, Z., Cheng, L., Gouretski, V., Zhang, B., Wang, Y., Li, F., Liu, Z., Zhu, J.: A new automatic quality control system  
629 for ocean profile observations and impact on ocean warming estimate, *Deep-Sea Res. Part I:*  
630 *Oceanographic Research Papers*, 194, <https://doi.org/10.1016/j.dsr.2022.103961>, 2023.
- 631 Tengberg, A., Hovdenes, J., Andersson, H. J., Brocandel, O., Diaz, R., Hebert, D., Americh, T., Huber, C., Körtzinger,  
632 A., Khripounoff, A., Rey, F., Rönning, C., Schimanski, J., Sommer, S. and Stangelmayer, A. : (2006):  
633 Evaluation of a lifetime-based optode to measure oxygen in aquatic systems. *Limnol. Oceanogr.: Methods*, 4,  
634 7-17, 2006.
- 635 Thierry, V., Bittig, H., and the Argo-BGC team: Argo quality control manual for dissolved oxygen concentration,  
636 Version 2.1, Argo Data Management, doi: <https://dx.doi.org/10.13155/46542>, 2021.
- 637 Uchida, H., Johnson, G. C., and McTaggart, K. E.: CTD Oxygen sensor calibration procedures. The Go-SHIP  
638 Repeat Hydrography Manual: A Collection of Expert Reports and Guidelines. IOCCP Report No. 14, ICPO  
639 Publication Series No. 134, Version 1, 17p., 2010.
- 640 WHPO: WOCE Operations Manual, Section 3.1.3: WHP operations and methods, WOCE report no. 69/91, WHPO 91-  
641 1. 80 pp., 1991.
- 642 Winkler, L.: Die Bestimmung des in Wasser gelosten Sauerstoffes. *Berichte der Deutschen Chemischen*  
643 *Gesellschaft*. 21 (2): 2843–2855. doi:10.1002/cber.188802102122, 1888.



- 644 Wunsch, C.: Towards the World Ocean Circulation Experiment and a bit of aftermath, Springer-Verlag, Jochum, M.,  
645 Murtugudde, R., Phys. Oceanogr., 181-201, 2006.
- 646 Yang, J., Rahardja, S., and Fränti, P.: Outlier Detection: How to Threshold Outlier Scores?, AIIPCC '19: Proceedings  
647 of the International Conference on Artificial Intelligence, Information Processing and Cloud Computing,  
648 December 2019. Article No.: 37, p. 1–6 <https://doi.org/10.1145/3371425.3371427>, 2019.